Investigation of NV (–) centers and crystallite interfaces in synthetic single-crystal and polycrystalline nanodiamonds by optical fluorescence and microwave spectroscopy

V. Yu. Yu Osipov, N. M Romanov, K. V Bogdanov, François Treussart, C. Jentgens, And A Rampersaud

Investigation of NV^- centers and crystallite interfaces in synthetic single-crystal and polycrystalline nanodiamonds by optical fluorescence and microwave spectroscopy

V. Yu. Osipov,[1,8] N. M. Romanov,[2,3] K. V. Bogdanov,[4] F. Treussart,[5] C. Jentgens,[6] and A. Rampersaud[7]

[1]*A. F. Ioffe Physics and Engineering Institute, St. Petersburg, Russia*
[2]*Peter the Great Polytechnic University, St. Petersburg, Russia*
[3]*Lappeenranta University of Technology, Lappeenranta, Finland*
[4]*ITMO University, St. Petersburg, Russia*
[5]*ENS Cachan, Université Paris-Saclay, Orsay Cedex, France*
[6]*Microdiamant AG, Lengwil, Switzerland*
[7]*Columbus Nanoworks, Columbus, Ohio, USA*
[8]*e-mail: osipov@mail.ioffe.ru*

Three types of diamond nanoparticles with sizes from 5 to 1000 nm have been investigated, whose crystal lattices include nitrogen-vacancy (NV) centers: detonation nanodiamonds (DNDs), dynamic-synthesis polycrystalline diamonds, and static-synthesis single-crystal diamonds. The electron paramagnetic resonance spectra have been investigated, along with the luminescence and IR absorption spectra of these materials. The DND concentration of NV^- centers is 2.7 ppm and is highest for particles in the size range up to 7 nm. The concentration of NV^- centers in polycrystalline diamonds is an order of magnitude less and depends on the average size of the polycrystalline particles, reaching a maximum at 180 nm in the average size range. The luminescence is brightest in 100-nm par-ticles of synthetic Ib diamonds subjected to high-energy-electron irradiation and annealing. The latter with an NV^- concentration of around 4 ppm can be used as fluorescent markers at the nanolevel.

1. INTRODUCTION

Materials that consist of nanoparticles with a crystalline surface that allows them to reliably function with various molecular agents and magnetically and optically active atomic-scale markers are currently attracting the interest of more and more researchers and developers from applied institutes and industrial companies involved in creating new engineering materials for innovative informational applications. Detonation nanodiamonds (DNDs) with a mean particle size of 5 nm, characterized by unsurpassed chemical inertness, good biocompatibility, and the possibility of using them as a basis for creating various composite molecular systems and active molecular superstructures with predictable promising physicochemical properties are demanded as nanocrystalline precursors for a wide range of applications in engineering, material science, and biomedicine [1–3]. They were invented in the USSR, and their technological potential is not yet definitively known, because the list of possible applications is still expanding. Detonation nanodiamonds are fabricated at commercial scales by exploding a trinitrotoluol–hexogen mixture in a closed volume under conditions of negative oxygen balance, after which chemical methods are used to isolate the diamond component from the detonation mix formed in the explosion. The diamond lattice is assembled in this case under high pressures and temperatures during a time of the order of microseconds from the carbon of the explosive compounds and fragmented submolecular structures of the compounds. The nitrogen of the explosion components causes substitutional nitrogen defects to be present in the diamond lattice, while the extremely rapid assembly of the diamond lattice of the nanocrystals during the detonation synthesis causes a high concentration of defects (including vacancies and multivacancies) in the diamond lattice. The nondiamond components are removed from the mix by processing it in aqueous nitric acid at temperatures

above 180°C, and the diamond particles are passivated by oxygen-containing atomic groups.

Another promising diamond product, polycrystalline diamond, fabricated in the process of shock-wave loading of a powdered graphite–copper mix, during which a direct graphite–diamond phase transition occurs, also possesses a number of unique properties and is available on the market. The method of synthesizing such polycrystals was developed by Western scientists in the mid-1970s and was subsequently successfully commercialized. The graphite-containing mix is rapidly loaded and compressed by detonating an explosive charge around a thick-walled steel tube that contains this mixture (so-called DuPont technology) that is accelerated from the outside by the energy of the explosion and collapses toward its longitudinal axis, while all the nondiamond components, including the construction metal that remains after the synthesis, is eliminated by chemical means [4–6]. The polycrystals thus formed consist of very densely bonded and randomly oriented 10–15 nm crystallites of cubic diamond [7]. The unusual properties of such a diamond product include higher mechanical strength and wear resistance of the submicrometer polycrystalline diamond particles than in a bulk diamond crystal or single-crystal diamond particles of the same size. Weak signals caused by $NV^{(-)}$ triplet centers were recently detected and identified by electron paramagnetic resonance (EPR) in both dynamic-synthesis materials[1] [8]. The specific EPR signals corresponding to $NV^{(-)}$ centers are caused by so-called forbidden $\Delta M_s = 2$ optical transitions (in the microwave region) between the Zeeman-split energy levels of the triplet state of the $S = 1$ center in a magnetic field [11,12]. It is remarkable in this case that no EPR signals corresponding to the allowed ($\Delta M_s = 1$) transitions are observed in triplet $NV^{(-)}$ centers in diamond nanoparticles with a size less than 20 nm. It is much harder to study the luminescence of these centers, since this requires elimination of stray effects associated with potential absorption of optical radiation by carbon in the sp^2 coordination. This paper is the first (to our knowledge) to compare studies by optical and EPR methods of $NV^{(-)}$ centers in DNDs and shock-wave-synthesized polycrystalline diamonds. In order to clarify the role of interfaces and intercrystallite boundaries in single particles or polycrystals, we study IR absorption in powders of the particles being analyzed. This is crucial because defects and intergrain boundaries that lie close to $NV^{(-)}$ centers can act as luminescence quenchants or can deactivate luminescence centers, including by the Förster mechanism of optical-excitation migration. The results are compared with those found for fluorescent 100-nm single-crystal nanodiamond particles obtained from microcrystals of synthetic high-pressure high-temperature (HPHT) Ib nitrogen-doped diamond by grinding, followed by irradiation with high-energy electron beams and annealing—i.e., specially fabricated samples that contain $NV^{(-)}$ centers.

[1]They are known as W15 centers in the traditional classification of paramagnetic defects in diamond. The W15 center was first observed in electron- or proton-irradiated type Ib diamonds by South African scientists (Loubser and Van Wyk) in 1977 [9]. The electron-level structure of this center was subsequently studied and described in detail in [10].

2. SAMPLES, MATERIAL-SYNTHESIS TECHNOLOGY, AND RESEARCH METHODS

This project involved fabricating and processing three different groups of nanodiamond materials with $NV^{(-)}$ centers unintentionally created in the material at the synthesis stage or created after synthesizing the crystallites but now on purpose. The processes had the purpose of promoting either the appearance of luminescence from the $NV^{(-)}$ centers or the detection of specific EPR signals from the $NV^{(-)}$ centers on the background of broad EPR signals from iron-containing complexes and compounds.

Different fractions of polycrystalline diamond powders from Van Moppes & Sons (Geneva, Switzerland) with a mean size that varied from 25 to 1000 nm were selected as the basic test material. Differently sized fractions were obtained by grinding large polycrystalline diamond particles with a size from 10 to 50 μm, produced using the DuPont technology, and then isolating a fraction of the particles with a mean size of 2–3 μm, after which the particles of this fraction were separated into submicrometer fractions by sedimentation in an aqueous medium and high-speed centrifugation.

Powders of the fine fractions were given additional chemical purification in mixtures of hot acids, using the equipment[2] of the Microdiamant Co. (Lengwill, Switzerland) and ENS Cachan (Université Paris-Saclay, France), in order to remove the graphite-like light-absorbing sp^2 phase around the polycrystalline particles and the $3d$ metallic impurities, mainly iron, that got into the material at the synthesis stage. The purity was monitored by x-ray fluorescence analysis. The purity was also monitored from the absence of a broad EPR signal from iron-containing complexes and iron compounds in the magnetic-field region corresponding to EPR signals with g-factor 4. The latter is a necessary but not sufficient condition for recording weak EPR signals with g-factor $g = 4.26$ from $NV^{(-)}$ centers. Lyophilic powders of gray color are obtained as a result of hot acid processing. The polycrystalline diamond powders purified in acids are designated in what follows as PCD-i, where index i (from 1 to 9) corresponds to fractions of different size ranges. Data on the different fractions of the PCD powders are indicated in Table 1.

The chosen comparison sample was DND powder produced by Special Technical Design Office Tekhnolog (St. Petersburg, Russia) and processed with aqueous nitric acid in an autoclave at 220°C–235°C, repeatedly rinsed in de-ionized water, and then dried. Primary drying was carried out at a temperature (no greater than 350°C) high enough to remove sorbed molecular groups but insufficient to gasify the carbon-containing fragments from the surface. This material, with a surface precoated with oxygenated groups, is then designated as DND-ox. The graphite-like phase in DND-ox was removed by oxidizing it and gas-phase etching in an oxygen-containing air atmosphere in a laboratory furnace at a fixed temperature chosen in the range from 420°C to 480°C for 12 h. About 50 mg of the DND-ox powder was held in the furnace during each heat treatment. The fall-off of the mass at temperatures

[2]Besides general-purpose chemical equipment, laboratory autoclaves with microwave heating (Anton Paar GmbH, Germany) were used.

Table 1. Particle and Crystallite Sizes in Different Powder Fractions of Single-Crystal and Polycrystalline Nanodiamonds

Marking of Nanodiamond Powders	Range of Particle Sizes, μm	Mean Size of Crystallites and/or Polycrystalline Aggregates in Powder, nm
Polycrystalline diamond		
PCD-1	0–0.05	25[a] (7–9)[b]
PCD-2	0–0.10	50[a] (7–9)[b]
PCD-3	0–0.15	75[a] (7–9)[b]
PCD-4	0–0.20	90[a] (7–9)[b]
PCD-5	0–0.35	180[a] (7–9)[b]
PCD-6	0–0.50	230[a] (7–9)[b]
PCD-7	0.25–0.50	350[a] (7–9)[b]
PCD-8	0.5–1.00	750[a] (7–9)[b]
PCD-9	0.75–1.25	1000[a] (7–9)[b]
Detonation diamond		
DND	≤ 0.050	4.5[b]
Synthetic HPHT Ib diamond		
FND-1	0–0.20	100[c]
FND-2	0–0.20	100[c]

[a]Manufacturer's data: for all fractions, the width of the particle-distribution function over sizes is of the order of the mean size of the polycrystalline particles.

[b]Size of the x-ray coherent-scattering region.

[c]Scanning-electron-microscope data for the crystallites.

above 480°C (for the DND-ox) was recorded, and the powder remaining after this processing was studied by IR spectroscopy.

Particles of fluorescent nanodiamonds (FNDs) with a mean size of 100 nm were used as material with specially induced $NV^{(-)}$ centers. These were obtained from synthetic (with atomic nitrogen impurities) microcrystalline HPHT Ib diamond with grain size 150 μm. The latter was first subjected to intense comminution to the submicrometer level, and the isolated superfine fraction was then irradiated in a thin layer with a beam of high-energy (5-MeV) electrons and was annealed in an inert atmosphere at 800°C. Here high-energy irradiation was used to create vacancies in the diamond lattice, and the subsequent annealing caused the vacancies to diffuse in the lattice and caused them to be captured on isolated nitrogen impurities (C defects). The nitrogen concentration in the microcrystal–precursors was 150 ppm (parts per million). The current in the electron beam was 25 mA. The minimum irradiation dose was 7.0×10^{18} electrons/cm^2. The electron-irradiated materials with exposures that differed by a factor of 2 (16 and 32 h) were then designated as FND-1 and FND-2. A fraction with a mean size of 100 nm was extracted using centrifugation in an aqueous medium. The FND powders were fabricated and supplied by Columbus Nanoworks Co. (Columbus, Ohio, USA).

Table 1 shows the marking of all the test samples of powders of polycrystalline, detonation, and ground single-crystal diamonds corresponding to the mean size of the individual particles and the ranges of variation of particle sizes in these powders.

The EPR spectra of the samples were recorded at room temperature in the X-range by means of an Elexsys E-680X Bruker EPR spectrometer at a frequency of 9.4 GHz. A quantity of 50–60 mg of the powder was poured into a clear fused quartz (CFQ) tube (Wilmad quartz EPR tubes, Sigma-Aldrich) 4 mm in outer diameter, having a powder column in the tube no more than 12 mm high. The open end of the tube was sealed against moisture. The tube with powder was fixed in the chamber of the microwave cavity. Spectra of EPR signals with g-factors in the range 4.00–4.30 were recorded at a microwave radiation power in the range 0.2–2 mW, modulation amplitude 3–10 G, magnetic-field modulation frequency 100 kHz, number of signal accumulations 1–50, chosen for weak signals from the optimum SNR conditions for recording. The time constant for one discrete reading was 0.020 s, and the total time was 100 s to record the spectrum for one pass in the magnetic-field sweep interval from 1300 to 2000 G. At microwave powers $P_{MW} < 4$ mW, the intensity of an EPR signal with a g-factor of $g \approx 4$ followed the linear dependence $I_{pp} \approx (P_{MW})^{1/2}$ in the detonation and polycrystalline diamonds, and no signal-shape distortions from saturation were recorded. The concentrations of paramagnetic $NV^{(-)}$ centers in the test samples were estimated by double integration of the corresponding EPR signal ($g = 4.26$) and the ratio of the measured value to the weight of the sample. Detonation nanodiamond powder with a known concentration of paramagnetic $S = 1/2$ centers equal to 6.3×10^{19} g^{-1} was used as a standard [13].

The secondary-emission spectra, which consists of luminescence radiation, along with Raman scattering, were recorded by means of an inVia μ-Raman apparatus (Renishaw, UK), using exciting laser radiation at a wavelength of 532 nm (or 488 nm)[3] and a 50× microscope lens that focuses the radiation into a spot about 2 μm in diameter on the surface of the sample. The secondary radiation was collected from the surface of the sample in the reverse-scattering geometry. A sample was fabricated for luminescence studies by pressing the powder into a cylinder 3 mm in diameter and no more than 2 mm thick inside a metallic holder. Fluorescence images of the brightest particles deposited from a droplet of the aqueous suspension were obtained by means of a Nikon Eclipse TiS epifluorescence inverted microscope using a Texas Red Cube standard optical filter (excitation 540–580 nm, transmitting 600–660-nm radiation), which transmits the main part of the emission from the $NV^{(-)}$ centers. The images are obtained with a 10 ms exposure by means of a 10× microscope lens.

Optical transmission spectra in the 700–4000 cm^{-1} region were recorded by means of a Specord-M80 two-beam IR spectrophotometer (Carl Zeiss, Jena, Germany). Powder of the test substance was pressed into a matrix of Uvasol spectroscopic-quality potassium bromide (CAS# 7758-02-3) (Merck, Darmstadt, Germany) under forevacuum pumping conditions. The weight concentration of the test substance in the dry mixture used for pressing was about 1:1000 or 4:1000 and was selected to optimize the modulation of the bands and lines with the highest absorption on the transmission spectra (dips all the way to 30%–50% of the maximum transmission level of the matrix). The spectra were recorded with a 2 or 4 cm^{-1} step. The time constant was chosen to equal 30 or 60 s. To obtain

[3]Exciting radiation with wavelength 488 nm was used only when studying the secondary-emission spectra of nanoparticles of polycrystalline diamond PCD, where the number of observable luminescence bands reached four or five.

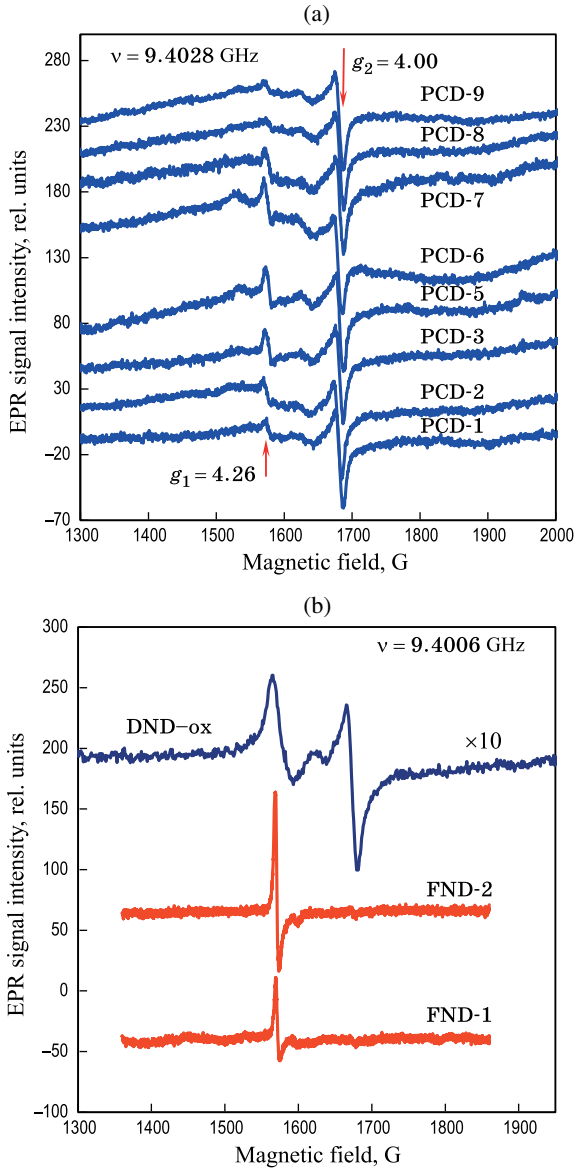

Fig. 1. (a) EPR spectra of different size-fractions (PCD-1–PCD-9) of dynamic-synthesis polycrystalline diamond and (b) detonation nanodiamond DND-ox and fluorescent synthetic HPHT Ib diamond (FND-1, FND-2) with mean particle size 100 nm. The size-fractions of the PCD polycrystals are designated on each spectrum in (a). The spectra in (a) are normalized to the intensity of the high-field EPR line with g-factor $g_2 = 4.00$ (from multivacancies). The microwave frequency is 9.40 GHz.

the absorption spectra of the test material, the resulting experimental data were corrected to take into account the spectral transmission of a pressed pellet made from pure KBr and were recalculated.

3. EXPERIMENTAL RESULTS AND DISCUSSION

A. Microwave Spectroscopy

The EPR spectra of different size-fractions of polycrystalline diamond (PCD) and DND-ox powder are shown in Figs. 1(a) and 1(b) in the magnetic-field range from 1300 to 2000 G. The low-field EPR line with g-factor $g_1 = 4.26$ corresponds to $NV^{(-)}$ centers, while the high-field line[4] with g-factor $g_2 = 4.00$ corresponds to the multivacancies formed in the crystals at the dynamic-synthesis stage as a result of the aggregation of vacancies into linear clusters of small extent. The intensities of both EPR lines in the DNDs ($g_1 = 4.26$ and $g_2 = 4.00$) are about equal, and the lines themselves are relatively broad. They were first recorded 10–12 years ago [13] in the EPR spectra of DNDs thoroughly purified from 3d metals and were subsequently identified as forbidden ($\Delta M_s = 2$) microwave-field-induced transitions between Zeeman-split energy levels of the triplet state of centers with spin $S = 1$ [8]. The specific location of the lines on the magnetic-field scale and the features of their shape are determined by the individual parameters of the spin Hamiltonian, which describes the exchange interaction of individual spins of 1/2 within a triplet center of each type ($NV^{(-)}$ and multivacancy) in the crystal lattice [8]. As can be seen from Fig. 1(a), the intensity of the $g_1 = 4.26$ line strongly depends on the mean size of the polycrystals,

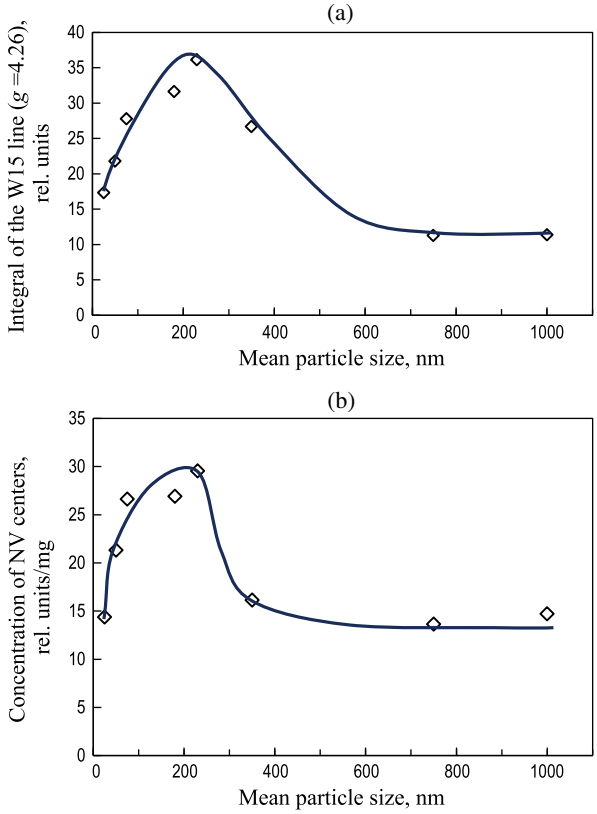

Fig. 2. (a) Peak intensity of the EPR line of the $NV^{(-)}$ centers with g-factor $g_1 = 4.26$ normalized to the intensity of the EPR line with g-factor $g_2 = 4.00$ and (b) the weight concentration of the $NV^{(-)}$ centers in the diamond polycrystals versus the mean size of the polycrystalline diamond aggregate.

[4]This line is separated from the low-field line by about 100 G on the magnetic-field scale and is clearly identified on the EPR spectra of not only all the size-fractions of the polycrystalline diamonds, but also of the DNDs.

whereas the overall ascending background and the intensity of the $g_2 = 4.00$ line show virtually no change in the series of PCD test samples. The corresponding size dependence of the intensity[5] of the $g_1 = 4.26$ line is shown in Fig. 2(a). It displays a pronounced maximum in the mid-range of sizes and a sharp falloff in the region above 350 nm. The weight concentration of $NV^{(-)}$ centers can be estimated by double integration of this line contour or as a product of the square of the line width ΔH_{pp} times its amplitude I_{pp}, after which this parameter is referred to as the mass of the powder. The spectra shown in Fig. 1(a) allow the $g_1 = 4.26$ lines of different amplitudes to be processed in this way. The concentration of $NV^{(-)}$ centers increases approximately linearly as the mean size of the polycrystals increases from 25 to 90 nm and reaches a maximum at 180–230 nm, after which it strongly falls off in the interval to 1000 nm [Fig. 2(b)]. The concentration of $NV^{(-)}$ centers is about 0.3 ppm at the maximum (for the PCD-6 fraction). The multivacancy concentration, determined by double integration of the high-field EPR line with g-factor $g_2 = 4.00$, remains approximately constant and shows virtually no dependence on the size of the polycrystals in the interval from 25 to 1000 nm. Such an observation was also pointed out in [14]. This can be indirect evidence not only of a reduction of the fraction of $NV^{(-)}$ centers in the material when there is a transition to small particles in connection with the breakdown of the centers in mechanically damaged regions of the lattice close to the outer surface but also of enrichment of the polycrystalline particles with nitrogen and not with vacancies for fractions of particles with a mean size in the range from 25 to 180 nm, possibly caused by the morphological features of the formation of large polycrystalline aggregates during shock-wave loading, after which they are separated into submicrometer fractions. The sections of the lattice that contain more impurity nitrogen are usually less mechanically strong and easily split apart from larger particles during grinding or even break down into still finer fragments. The width of the EPR lines ($g_1 = 4.26$) for $NV^{(-)}$ centers in polycrystals of all the size-fractions PCD-1 to PCD-9 are about the same, but less than for DND-ox. The $g_1 = 4.26$ line is about 13 G wide in DND-ox, while it is about 8–9 G wide in PCD. (The EPR high-field $g_2 = 4.00$ line is also about 8–9 G wide in PCD powders and is virtually independent of the mean size of the polycrystals.) On the assumption that the $g_1 = 4.26$ EPR line undergoes dipole–dipole or exchange broadening, this indicates a substantially larger spacing from the isolated $NV^{(-)}$ centers with spin $S = 1$ in the diamond lattice to the closest paramagnetic $S = 1/2$ centers (broadening agents) at the intergrain boundaries and/or the crystallite interfaces in PCD than in DND-ox. This is very reasonable, taking into account that the mean crystallite size equals 10–15 nm in PCD and 4.5 nm in DND-ox. The probable conditions for luminescence quenching thus look much less rigorous in PCD than in DND-ox, where the crystallite boundary gets much closer to the radiative luminescence center inside the nanoparticle. The concentration of $NV^{(-)}$ centers in DND-ox in this case is estimated as approximately 2.7 ppm, which is more than sufficient in practice to obtain bright luminescence from the nanoparticles, provided luminescence-quenching processes are neglected. There is one $NV^{(-)}$ center for thirty 5 nm DND particles in this case, and this is insufficient for the individual 5-nm particles to be used as separate luminescence markers. However, the 30–35 nm DND aggregates that are most stable in aqueous solutions and which consist of more than a hundred individual nanoparticles always contain several $NV^{(-)}$ centers and are suitable for marking at the submicrometer level.

The EPR spectra of the FND-1 and FND-2 samples with an irradiation dose by high-energy electrons that differs by about a factor of 2 are shown in Fig. 1(b). It can be seen that, in a magnetic field that is half as strong,[6] the spectra contain only the characteristic narrow $g_1 = 4.26$ line from $NV^{(-)}$ centers of different amplitudes, approximately proportional to the irradiation dose, but there are no signals from multivacancies or other triplet centers [Fig. 1(b)]. The EPR signal with g-factor $g_1 = 4.26$ (from the $NV^{(-)}$ centers) is absent from the original nonirradiated HPHT Ib crystal in this case, and this is evidence that $NV^{(-)}$ centers appear in the crystals only after they are irradiated with high-energy electrons and annealed. At the same time, unlike the DND and PCD materials with small crystallites (about 5 and 10–15 nm across), the FND-1 and FND-2 EPR spectra demonstrate a strong signal from P1 centers (substitutional nitrogen) in the 3240–3460-G magnetic-field region with resolved superfine structure, associated with magnetic interaction of the unpaired antibonding orbitals of the P1 center with the nuclear magnetic moment of the nitrogen atom.[7] The central $g = 2.0024$ line, with symmetric low- and high-field satellites separated by 60 G on the magnetic-field scale, is the characteristic signature of P1 centers. This is evidence of the high quality of the specially fabricated FND particles with substitutional nitrogen impurities in which the concentration of all the paramagnetic defects with spin 1/2 does not exceed 130 ppm. At the same time, an analysis of the overall intensity of the $g_1 = 4.26$ line is evidence that the concentration of fluorescent $NV^{(-)}$ centers in FND-2 is about 4 ppm. The EPR method can thus be used for an independent estimate of the concentration of $NV^{(-)}$ centers in fluorescent diamonds smaller than 100–150 nm, where these centers were unintentionally created (during synthesis) or specially created (by electron-beam irradiation after synthesis).

B. Luminescence Properties

The secondary-emission spectra of polycrystalline diamonds PCD-2, PCD-4, and PCD-5 with a mean polycrystal size of 50, 90, and 180 nm and DND-ox powder processed in air at 430°C are shown in Figs. 3(a) and 3(b). The DND-ox luminescence spectrum with a maximum at 678 nm is

[5]The peak intensity I_{pp}—i.e., the distance between the maximum and minimum along the vertical on the spectrum of the first derivative—is implied from the microwave absorption.

[6]This refers to a magnetic-field region in which there are weak EPR signals with a g-factor of $g \approx 4$ and its neighborhood. This actually occurs in magnetic fields that are half as great as those in which the main EPR signal is observed for nanodiamonds with a g-factor of $g = 2.0024$–2.0027.

[7]The EPR spectrum of this signal in the 3240–3460-G region is not shown here, since the form of the signal is standard, with typical triplet superfine structure.

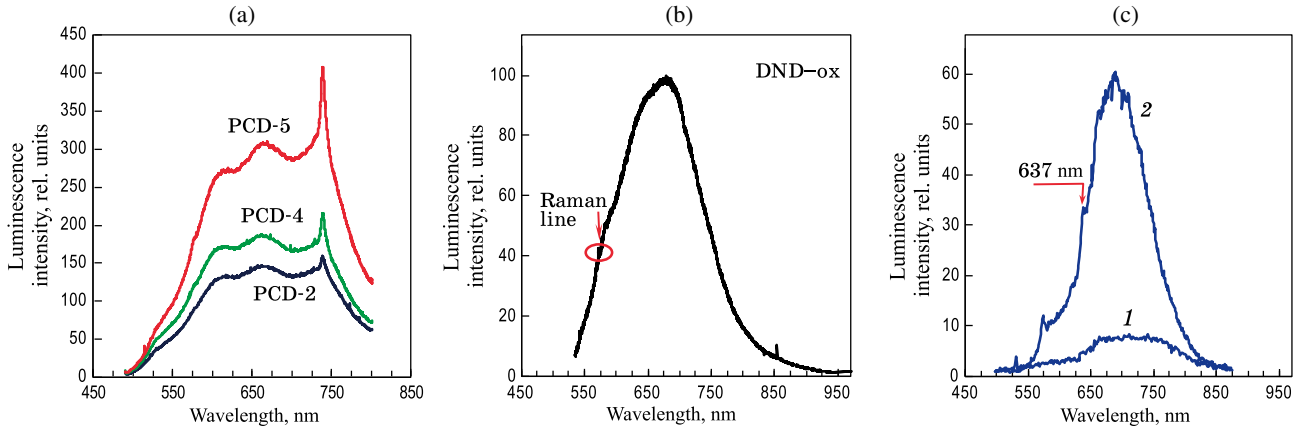

Fig. 3. Secondary-emission spectra of nanodiamond particles with $NV^{(-)}$ centers in materials of different synthesis and processing types. (a) Polycrystalline diamond (PCD-2, PCD-4, PCD-5) with a mean aggregate size of 50, 90, and 180 nm; (b) DND-ox; and (c) FND-1 (*1*) and FND-2 (*2*). The spectra were excited by laser radiation at (a) 488 nm and/or at (b), (c) 532 nm.

predominantly associated with the radiation of $NV^{(-)}$ centers [Fig. 3(b)]. The wide emission band that stretches to 770 nm or further is associated with multiple (usually up to eight) phonon sidebands [10], as occurs in micrometer-size single crystals. The background band in this case is 700 meV wide on the energy scale [10] (at the 5% level of the maximum intensity). Since the mean DND-ox particle size is 4–5 nm, and the phonon-confinement effect is substantial under these conditions, the fine structure of the phonon wing of the emission spectrum (with several characteristic peaks) is not spectrally resolved. The position of the Raman line of diamond[8] in DND-ox particles is shifted by 8–10 cm^{-1} relative to the corresponding value for bulk diamond (1332 cm^{-1}) because of the phonon-confinement effect and equals 1324 cm^{-1}, while the line width at half-height is about 25 cm^{-1}. In turn, the luminescence spectra of very different fractions of polycrystalline diamonds (PCD-2, PCD-4, and PCD-5) demonstrate several characteristic bands (up to four or five) that are easily separated and identified by resolving the spectra into Gaussian contours or mixed Gaussian–Lorentzian types [Fig. 3(a)]. One of these, a narrow long-wavelength band centered at 739 nm, is associated with SiV centers, while another, moderately wide band with a maximum at 663 nm is associated with $NV^{(-)}$ centers. The latter attribution is based on the fact that EPR spectroscopy shows that an appreciable number of $NV^{(-)}$ centers are present in the material. One more wide photoluminescence band is the most intense band and lies in the short-wavelength region, with its maximum at 610 nm; it may be associated with emission from $NV^{(0)}$ centers. The green luminescence band with maximum at 525 nm is most likely associated with emission from NVN (or H3) centers. These bands were first detected and some of them (at 739 nm) were described in detail in [15]. The intensities of both red luminescence bands may be directly associated with the number of NV centers in neutral and negatively charged states, the latter of which are easy to detect by means of EPR. For polycrystal particles with a mean size in the range from 25 to 230 nm, good correlation is observed between two of these parameters—the luminescence intensity in the 600–750 nm band and the $NV^{(-)}$ concentration determined by EPR. The red luminescence band is most intense for polycrystal fractions with a mean size of 180 nm and/or 230 nm.

The secondary-emission spectra of FND-1 and FND-2 obtained with excitation by 532 nm laser radiation demonstrate characteristic wide luminescence bands associated with emission from $NV^{(-)}$ defects [Fig. 3(c), lower (*1*) and upper (*2*) spectra]. In this case, for material with a short exposure time by high-energy electrons (FND-1) and a correspondingly low concentration of $NV^{(-)}$ defects, the luminescence band has virtually no structure in the interval from 600 to 820 nm. In turn, the material with twice the exposure time (FND-2) and a larger concentration of $NV^{(-)}$ defects demonstrates fine features in the luminescence spectra, including a zero-phonon line at 637 nm and a band in the 650–820 nm range associated with phonon side bands. The luminescence intensity of FND-2 in this case turns out to be a factor of 7–8 higher than that of FND-1. The fluorescence image of a dried droplet of a suspension of FND-2 nanoparticles obtained using the Texas Red Cube filter, which transmits radiation in the 600–660 nm interval, is shown in Fig. 4. It has the shape of a narrow luminous red ring, where the precipitated material formed during the specific drying of the water droplet has its maximum concentration. The superior fluorescence characteristics of FND-2 have two simultaneous causes—a high concentration of artificially created $NV^{(-)}$ centers, which reaches 4–5 ppm, and high optical quality of the diamond lattice in individual particle–crystals, with a mean size of 100 nm obtained by grinding. The number of defects induced by grinding in the lattice and in the mechanically disturbed region close to the surface of the particles is negligible for quenching the luminescence from the overwhelming number of $NV^{(-)}$ centers inside such 100 nm particles. The fluorescence characteristics (spectral composition, luminescence intensity) are about the same in specially irradiated and annealed synthetic micrometer-size HPHT crystals of Ib diamond [16].

[8]The position of the Raman line of diamond is denoted by an arrow on the secondary-emission spectrum in Fig. 3(b).

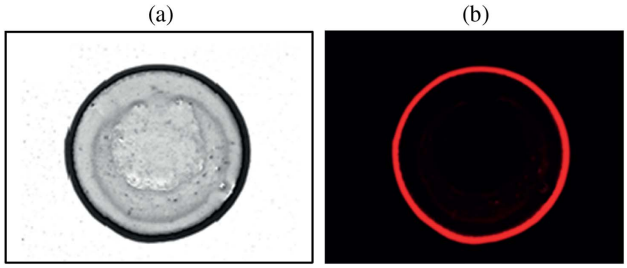

Fig. 4. (a) Optical image of a dried drop of an aqueous suspension of FND-2 synthetic diamond nanoparticles with $NV^{(-)}$ centers and (b) the corresponding fluorescence image of the drop, obtained using an epifluorescence microscope, a Texas Red Cube red filter (600–660 nm), and an illuminating laser with wavelength 532 nm. The observed red ring corresponds to the sections on the substrate in which the concentration of precipitated FND-2 particles is greatest when the sample dries out. The ring is 0.8–0.9 mm in diameter.

In the PCD polycrystals studied in this paper, the $NV^{(-)}$ centers are located in 10–15 nm crystals, with several (as many as three or four) crystallites on the average for every $NV^{(-)}$ center. A model of polycrystals with $NV^{(-)}$ centers is shown in Fig. 5(a). The $NV^{(-)}$ centers close to the outer boundaries of the polycrystals are more favorably located in principle from the viewpoint of emitting radiation than the centers deep inside large polycrystals. However, effects induced by grinding and cracking the original large polycrystalline particles along intergrain boundaries can also deactivate the $NV^{(-)}$ centers that lie close to the outer surfaces of the polycrystals, including by reversing their electrical charge or even by destroying them. This may have the result that the weight concentration of $NV^{(-)}$ centers smoothly decreases as the average particle size decreases from 180 to 25 nm according to the EPR spectroscopy data.

It is clear that high luminescence output from materials that contain $NV^{(-)}$ centers can be ensured by reducing the absorption of the radiation emitted at the surfaces and grain boundaries of the particles, particularly those that contain graphene-like sp^2 fragments of various thicknesses. The presence of sp^2-hybridized carbon in PCD polycrystals was demonstrated by Raman spectroscopy [15] and is also confirmed

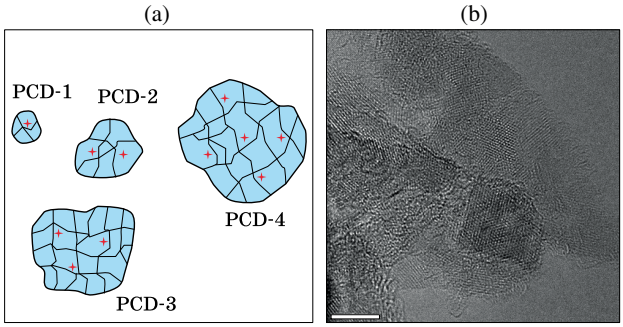

Fig. 5. (a) Diagram of the structure of polycrystalline diamond particles of different size-fractions and (b) an image of PCD-1 polycrystals with mean size 25 nm, obtained by high-resolution transmission electron microscopy. The red crosses schematically show the positions of the $NV^{(-)}$ centers in the individual crystallites of the polycrystal. The scale strip on the right-hand panel is 4 nm wide.

by high-resolution transmission electron microscopy. One way to eliminate graphene-like fragments from the crystallite surface is by selective liquid-phase (in acids at high temperatures) or gas-phase oxidation of the surface, so that easily oxidized components are eliminated in the liquid-phase or gas-phase processes. Many materials, including DND-ox and PCD, become luminescent as a result of such auxiliary processing. We shall consider the IR absorption characteristics of materials that undergo such oxidative processing.

C. Infrared Absorption

Figure 6(a) (curve *1*) shows the IR absorption spectrum of sample PCD-1 after final processing in mixtures of acids. This spectrum contains a broad structureless band in the 1000–1300 cm^{-1} interval, predominantly associated with vibrational absorption of C–O and C–O–C groups on the surfaces of the crystallites that compose the polycrystals and two narrow bands in the neighborhood of 1630 cm^{-1} and 1800 cm^{-1}, associated with the absorption and valence vibrations of hydroxyl and carbonyl groups [17,18]. A pronounced band from the carbonyl groups appears at 1800 cm^{-1} in the absorption spectra of the processed material [Fig. 6(a), curves *1–4*] as a result of acid processing of the polycrystalline PCD samples of all the smallest size-fractions (less than 200 nm) in an autoclave. However, all the features in the 900–1500 cm^{-1} interval of the wide absorption band of the various fractions of the materials subjected to acid processing are maintained after processing—even the details of the bands at 1100 and 1200 cm^{-1}. This means that the primary functional groups that appear on the inner and outer interfaces of the polycrystals at the synthesis and extraction stages are inert and stable against chemical processing in mixtures of acids in an autoclave at 170°C. The absorption band at 1100–1110 cm^{-1} is present on the IR spectra of the PCD-1–PCD-4 samples of all the smallest size-fractions obtained by separation and fractionation in an aqueous medium, showing that C–O and C–O–C groups are present both on the outer surface of the polycrystals and on the inner interphase boundaries. The absorption band at 1100–1110 cm^{-1} has different intensities in the polycrystals of the different size-fractions and is a maximum for the PCD-4 polycrystal fraction. Spectra *1–4* in Fig. 6(a) are normalized to the intensity of the peak at 1800 cm^{-1}, which is associated with vibrations of the carbonyl groups that result from chemical processing on the outer surface of the polycrystals—i.e., those exposed only to external agents. This means that the carbonyl groups enter into the composition of the carboxyl or anhydride groups on the surface of the polycrystals, while the C–O–C groups are fragments of a different type of atomic structures associated with the internal and external interfaces (by analogy with the model of [19] for DND aggregates). The internal interfaces that separate the crystallites in the polycrystals can also contain island-type graphite-like interlayers of atomic thickness. The intensity ratio of the absorption peaks at 1110 and 1800 cm^{-1} (I_{1110}/I_{1800}) is approximately proportional to the size of the polycrystalline particles in the interval from 25 to 100 nm. This means that C–O and C–O–C groups are present in the inner volume of the polycrystalline particles on the intercrystalline interfaces. The presence of covalent C–O/C–O–C bonds at the grain

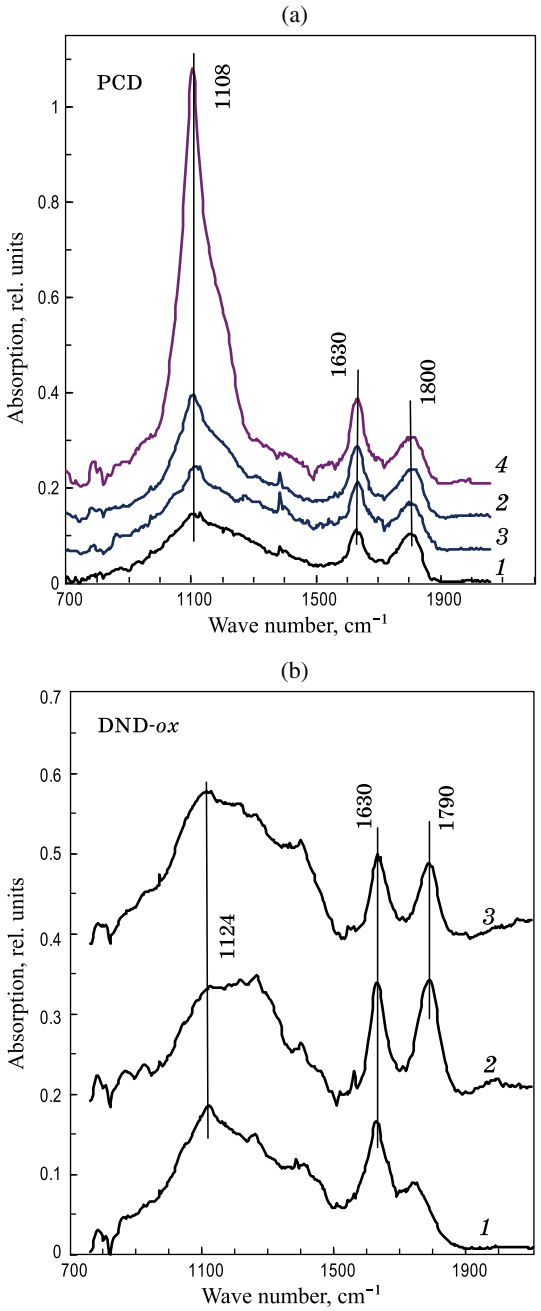

Fig. 6. Infrared absorption spectra of (a) the smallest size-fractions of polycrystalline diamond, formed in mixtures of acids in an autoclave and (b) detonation diamond DND-ox heat-treated in air. (a) shows the following size-fractions: *1*—PCD-1, *2*—PCD-2, *3*—PCD-3, *4*—PCD-4. (b) shows the following process temperatures in °C: *1*—350, *2*—430, *3*—520. For simplicity, the two groups of spectra are shifted vertically by (a) 0.07, 0.14, and 0.21 and (b) 0.2 and 0.4 scale units, respectively.

boundaries and interfaces between the crystallites, apparently densely sintered and bonded to each other during the shock-wave synthesis, explains the excellent stability of the polycrystalline particles of PCD against chemical processing in acids at temperatures all the way to 190°C. It is assumed here that the oxidizing chemical agent does not penetrate inside the polycrystals along the intergrain boundaries and interfaces between the crystallites. At the same time, it is impossible to completely rule out that the absorption peak at 1110 cm^{-1} is associated with valence vibrations in C–N groups. The absorption band with a peak at 1110 cm^{-1} is relatively wide and contains a high-frequency wing (rise), which is obviously formed as a result of a second, nearby band (contour) alongside, with center at 1200 cm^{-1} [Fig. 6(a), curve *4*]. Additional Gaussian-type contours that strongly overlap with the bands at 1100 and 1200 cm^{-1} may lie between them in the range from 1100 to 1200 cm^{-1}. As is well known, substitutional nitrogen defects cause an absorption line at 1130 cm^{-1} in bulk nitrogen-doped diamond crystals (C defects) in the concentration range from 100 to 2000 ppm or even higher [20]. However, in the case of the internal intergrain boundaries (interfaces) between the crystallites in the polycrystals, a significantly greater amount of atomic nitrogen can be contained on the boundaries of these crystallites, saturating all the broken bonds that are present there and participating in the structure of the different configurations of strong C–N–C links between the crystallites. Such a possibility cannot be ruled out, considering that nitrogen was incorporated into the lattice at the synthesis stage when $NV^{(-)}$ centers were formed. As is well known, Si–O bonds can also give strong absorption peaks at 1100 cm^{-1} if an amorphous SiO_x phase is present around the diamond nanocrystals [21]. However, the amount of silicon available in the sample (it is proven in [15] that silicon and SiV defects are present) is clearly insufficient in our case to explain the presence of strong absorption bands at 1100 cm^{-1} in the polycrystalline diamonds of the small size-fractions (PCD-1–PCD-4). The silicon concentration is less than 100–140 ppm in all the size-fractions of factory-processed polycrystalline diamond and is already less than 10–12 ppm in chemically purified powders.

The IR absorption spectrum of the reference DND sample of interest (DND-ox) is shown for comparison in Fig. 6(b) (spectrum *1*). It is very similar in appearance to the IR absorption spectrum of the PCD-1 polycrystalline diamond sample considered above. The combined band at 1630 cm^{-1} is associated with valence vibrations of the hydroxyl groups of water molecules sorbed on the surface of the DND particles or in the potassium bromide matrix and is not eliminated from it at the stage of pressing the mixture. The spectrum contains a wide structureless band of triangular shape in the interval 850–1500 cm^{-1}, which in the 1000–1300 cm^{-1} region is also predominantly associated with absorption at the vibrations of the C–O and C–O–C groups that are present on the surface of the particles and a small band of Gaussian shape in the neighborhood of 1740 cm^{-1}, associated with absorption at the valence vibrations of carbonyl groups. The given absorption is characteristic of DND processed in acids and was mentioned earlier in [22] and [23]. In the wide 850–1500 cm^{-1} band, at least five overlapping absorption bands of Gaussian shape can be distinguished at 970, 1050, 1120, 1250, and 1400 cm^{-1}. Three of these peaks (at 1050, 1120, and 1250 cm^{-1}) are apparently fundamental characteristics of the oxidized surface of diamond and were observed earlier in the absorption spectra of variously processed detonation nanodiamonds [22,23]. A peak

with maximum at 1100–1130 cm^{-1} was pointed out in virtually all papers on the IR spectroscopy of DND.

Figure 6(b) also shows the absorption spectra of the DND-ox reference sample subjected to heat treatment in air. Spectra *2* and *3* in Fig. 6(b) are evidence of substantial changes in the composition of the functional groups on the surface of isolated DND-ox nanoparticles or aggregates as a function of the processing temperature in air. The absorption zone at 1100–1130 cm^{-1} is also present on the spectrum of DND-ox, as it is in PCD-1 and is evidence of the presence of C–O and C–O–C groups both on the outer surface of the DND particles and on the inner boundaries in DND aggregates with a mean size of 30 nm. In the interval of treatment temperatures from 350°C to 520°C, the absorption spectra of DND-ox (spectra *2* and *3*) includes an absorption band at 1780–1790 cm^{-1} from carbonyl groups. It forms when diamond undergoes dry or moist surface oxidation in air. The 1780–1790 cm^{-1} absorption peak from carbonyl groups is already substantially decreased at $t \geq 550$°C (by a large factor; the spectrum is not shown on the figure), and this is associated with gas-phase etching of the surface and ablation of the material. The latter is most distinctly seen and has the greatest intensity at temperatures of 430°C–520°C [Fig. 6(b), spectra *2* and *3*], and this is evidence that carbonyl groups are prevalent on the surface in this range of heat treatment. The highest luminescence intensity of the $NV^{(-)}$ centers is demonstrated by DND particles subjected to such treatment, which are optimal for applied uses regardless of their morphological status—isolated 5-nm particles or aggregates with a mean size of 30–35 nm. The changes that occur when $t \geq 550$°C are associated with surface etching of the particles, ablation of the material by volatile reaction products of oxidation, and the appearance of a family of functional groups of another composition on the DND surface [24].

4. CONCLUSION

It has thus been demonstrated that the EPR method is extremely effective for estimating the concentration of $NV^{(-)}$ centers in synthetic fluorescent nanodiamonds, where these centers appeared at the synthesis stage or were later specially created. For particles in the size range up to 7 nm, the greatest concentration of $NV^{(-)}$ centers (2.7 ppm) is reached in detonation diamonds; however, because of the total defect content of the crystal lattice of particles of DND and its surface, the luminescence intensity is low because of different types of quenching effects. Nevertheless, each 30–35-nm aggregate consisting of densely sintered DND particles contains from two to five $NV^{(-)}$ centers and is optically recorded individually. Dynamically sythesized polycrystalline diamond particles also display $NV^{(-)}$ luminescence. Their $NV^{(-)}$ concentration is less than that of DND. However, the concentration of $NV^{(-)}$ centers and the luminescence intensity from the $NV^{(-)}$ centers are greatest in polycrystalline diamonds whose aggregates have a mean size of 180 nm. The effective concentration of $NV^{(-)}$ centers in smaller polycrystalline aggregates is lower because of deactivation effects of the centers by surface effects or because they break down in the mechanically damaged surface layer. Specially irradiated and annealed synthetic fluorescent HPHT Ib diamonds demonstrate a high concentration of $NV^{(-)}$ centers (up to 4–5 ppm) along with high quality of the crystal lattice; this is especially important for obtaining high-intensity fluorescence radiation from submicrometer (0.1 μm) particles and is best-adapted to technical and other applications. Fluorescent DND and FND particles can be used to create subsurface marks and markers in plastics, biopolymers, and polymeric composites that weakly absorb optical radiation in the 600–750 nm spectral range, especially in those regions where long-lived stability and thermal resistance of the luminescence centers is actually present under conditions of a chemically aggressive atmosphere or UV radiation.

Funding. Russian Science Foundation (RSF) (14–13–00795); Japan Society for the Promotion of Science (JSPS) (L17526); Russian Foundation for Basic Research (RFBR) (17-52-50004 YaF_a).

Acknowledgment. The authors are grateful to Professor Takuya Hayashi from Shinshu University (Nagano, Japan) for help in obtaining images of particles by high-resolution transmission electron microscopy. V. Yu. Osipov is grateful to Hosei University (Tokyo, Japan) for collaboration.

REFERENCES

1. A. Vul' and O. Shenderova, eds., *Detonation Nanodiamonds: Science and Applications* (Pan Stanford, Singapore, 2014).
2. V. N. Mochalin, O. Shenderova, D. Ho, and Y. Gogotsi, "The properties and applications of nanodiamonds," Nat. Nanotechnol. **7**(1), 11 (2012).
3. O. Shenderova and G. McGuire, "Science and engineering of nanodiamond particle surfaces for biological applications," Biointerphases **10**, 030802 (2015).
4. R. M. Hazen, "The new diamond makers: diamonds by explosion," in *The Diamond Makers* (Cambridge University Press, Cambridge, 1999), Chap. 11, pp. 190–198.
5. J. Beard, "Explosive mixtures," New Scientist (1637), 43–47 (1988).
6. L. N. Teasley, N. F. Bailey, and O. R. Bergmann, "Micropolycrystalline diamond by shock synthesis: advances in performance and property characterization," Proc. Electrochem. Soc. **97–32**, 48–57 (1998).
7. P. D. Ownby, "Nano 6H diamond polytype polycrystalline powder," NSTI-Nanotech. **3**, 210 (2004).
8. A. I. Shames, V. Yu. Osipov, H. J. von Bardeleben, and A. Ya. Vul', "Spin S=1 centers: a universal type of paramagnetic defects in nanodiamonds of dynamic synthesis," J. Phys. Condens. Matter **24**(22), 225302 (2012).
9. J. H. N. Loubser and J. A. van Wyk, "Electron spin resonance in the study of diamond," Rep. Prog. Phys. **41**, 1201 (1978).
10. M. W. Doherty, N. B. Manson, P. Delaney, F. Jelezko, J. Wrachtrup, and L. C. Hollenberg, "The nitrogen-vacancy colour centre in diamond," Phys. Rep. **528**(1), 1 (2013).
11. A. I. Shames, V. Yu. Osipov, H. J. von Bardeleben, J.-P. Boudou, F. Treussart, and A. Ya. Vul', "Native and induced triplet nitrogen-vacancy centers in nano- and microdiamonds: half-field electron paramagnetic resonance fingerprint," Appl. Phys. Lett. **104**, 063107 (2014).
12. A. I. Shames, V. Yu. Osipov, J. P. Boudou, A. M. Panich, H. J. von Bardeleben, F. Treussart, and A. Ya. Vul', "Magnetic resonance tracking of fluorescent nanodiamond fabrication," J. Phys. D: Appl. Phys. **48**(15), 155302 (2015).
13. V. Yu. Osipov, A. I. Shames, T. Enoki, K. Takai, M. V. Baidakova, and A. Ya. Vul, "Paramagnetic defects and exchange coupled spins in pristine ultrananocrystalline diamonds," Diamond Relat. Mater. **16**(12), 2035 (2007).

14. A. I. Shames, D. Mogilyansky, A. M. Panich, N. A. Sergeev, M. Olszewski, J.-P. Boudou, and V. Yu. Osipov, "XRD, NMR, and EPR study of polycrystalline micro- and nanodiamonds prepared by a shock wave compression method," Phys. Status Solidi A **212**(11), 2400 (2015).
15. K. V. Bogdanov, V. Yu. Osipov, M. V. Zhukovskaya, C. Jentgens, F. Treussart, T. Hayashi, K. Takai, A. V. Fedorov, and A. V. Baranov, "Size-dependent Raman and SiV-center luminescence in polycrystalline nanodiamonds produced by shock wave synthesis," RSC Adv. **6**, 51783 (2016).
16. A. I. Shames, V. Yu. Osipov, K. V. Bogdanov, A. V. Baranov, M. V. Zhukovskaya, A. Dalis, S. S. Vagarali, and A. Rampersaud, "Does progressive nitrogen doping intensify negatively charged nitrogen vacancy emission from e-beam-irradiated Ib type high-pressure-high-temperature diamonds?" J. Phys. Chem. C **121**(9), 5232 (2017).
17. K. Iizuka, Y. Furukawa, and R. Oshima, "Analysis of binding state of heat treated diamond powder," Am. J. Chem. Mater. Sci. **1**(1), 7 (2014).
18. N. B. Colthup, L. H. Daly, and S. E. Wiberley, *Introduction to Infrared and Raman Spectroscopy* (Academic Press, New York, 1964).
19. K. Xu and Q. Xue, "New method for deaggregation of nanodiamond from explosive detonation: graphitization-oxidation method," Phys. Solid State **46**(4), 649 (2004) [Fiz. Tverd. Tela **46**(4), 633 (2004)].
20. A. M. Zaitsev, *Optical Properties of Diamond: A Data Handbook* (Springer-Verlag, Berlin, 2001).
21. I. Rehor, J. Slegerova, J. Kucka, V. Proks, V. Petrakova, M.-P. Adam, F. Treussart, S. Turner, S. Bals, P. Sacha, M. Ledvina, A. M. Wen, N. F. Steinmetz, and P. Cigler, "Fluorescent nanodiamonds: fluorescent nanodiamonds embedded in biocompatible translucent shells," Small **10**(6), 1106 (2014).
22. I. I. Kulakova, "Surface chemistry of nanodiamonds," Phys. Solid State **46**(4), 636 (2004) [Fiz. Tverd. Tela **46**(4), 621 (2004)].
23. Y. W. Zhu, X. Q. Shen, B. C. Wang, X. Y. Xu, and Z. J. Feng, "Chemical mechanical modification of nanodiamond in aqueous system," Phys. Solid State **46**(4), 681 (2004) [Fiz. Tverd. Tela **46**(4), 665 (2004)].
24. S. Osswald, G. Yushin, V. Mochalin, S. O. Kucheyev, and Y. Gogotsi, "Control of sp^2/sp^3 carbon ratio and surface chemistry of nanodiamond powders by selective oxidation in air," J. Am. Chem. Soc. **128**(35), 11635 (2006).